Characterizing mean and turbulent structures of hurricane winds via large-eddy simulations

By F. Sabet,† Y. R. Yi, L. Thomas AND M. Momen†

Hurricanes have been the most expensive and devastating natural disasters in US history. Nevertheless, our understanding of the turbulence processes in these flows is limited. Our objective in this study is to bridge this knowledge gap by conducting a thorough sensitivity analysis of the hurricane boundary layer using large-eddy simulations. We characterize the impacts of the radius, surface roughness, gradient wind, and sub-grid-scale viscosity models on the hurricane's mean and turbulence dynamics. Our results indicate that increasing the Rossby number (rotation) increases the hurricane's maximum jet velocity, reduces the boundary layer height, and decreases the size of coherent turbulent structures at the same elevation. This study provides insights into the turbulence dynamics in hurricanes and can guide the development of more accurate turbulence models for rotating hurricane flows.

1. Introduction

Global warming could increase the intensity and destructiveness of future hurricanes (Emanuel 2005). The primary circulation of a hurricane is driven by four major forces: pressure gradient, centrifugal, Coriolis, and friction. In the free atmosphere, friction is negligible; therefore, the remaining forces constitute a gradient wind balance. Near the surface, friction modulates the force balance and causes the wind to be angled inward toward the eye of the hurricane, creating an inflow. The dominance of these forces in a hurricane is typically determined by the non-dimensional Rossby number (Ro), which is defined as the ratio between the centrifugal and Coriolis forces. The strong rotational effects that exist in hurricane boundary layers (HBLs; $Ro \gtrsim 1$) make them distinctive compared with regular atmospheric boundary layers ($Ro \ll 1$).

Numerical simulations provide a powerful tool to understand and model the complex dynamics of hurricane flows. In recent years, the resolution of full hurricane simulations in weather models has decreased from a 5 km grid size to $\sim$1 km (Zhang et al. 2018). Nonetheless, the mechanisms of turbulent mixing in hurricane flows that include high wall-normal rotation are neither fully understood nor accurately predicted (Romdhani et al. 2022) because grid resolutions on the order of 10 m are required to resolve turbulent flow fields.

The large-eddy simulation (LES) technique provides a high-fidelity numerical framework that can bridge this knowledge gap by resolving turbulent eddies in hurricanes. Compared with conventional mesoscale weather models, the key advantage of LES is that the large energetic eddies are explicitly resolved and only the dynamics of small-scale, low-energy, isotropic eddies [i.e., the sub-grid-scale (SGS) motions] are modeled. As

† Department of Civil and Environmental Engineering, University of Houston

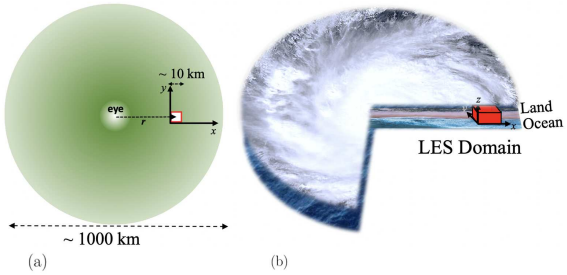

domain.pdf

FIGURE 1. (a) Schematic of a hurricane and (b) a selected portion as our LES domain. The shading in panel (a) displays the wind speed magnitude. The figure is from Momen et al. 2021.

of yet, no thorough sensitivity analysis of hurricane turbulence dynamics has been performed based on the HBL parameters such as the hurricane's radius, surface roughness, and radial velocity gradients. Our objective in this study is to address this knowledge gap by utilizing a novel high-fidelity LES solver to improve our understanding of HBL turbulence mechanisms and coherent structures. To this end, the main questions of this research are:

1) What are the impacts of rotation on HBL dynamics and its turbulence structures?

2) How do HBL mean and turbulence dynamics respond to changing the HBL parameters and SGS models in LES?

We answer these questions in the following sections using a suite of LESs by varying the simulated domain's distance from the hurricane center (20 km to 160 km), imposed geostrophic velocity profiles (various shapes and magnitudes), aerodynamic roughness length (from smooth to rough walls), and SGS models.

2. Formulation and computational setup

To simulate the HBL with centrifugal forces in the LES, we derived and validated a novel set of governing equations (Momen et al. 2021). The first main advantage of such a model is that, its resolution is much higher than that of many available simulations (see Figure 1), which allows us to resolve the turbulent cyclonic winds in greater detail ($\sim$10 m versus $\sim$1 km of weather models). Second, it differs from previous methods by leveraging an analytical treatment of the governing equations to simplify the analysis of the multi-scale structure of the HBL (Green & Zhang 2015).

The governing equations for the LES of HBLs can be written for the filtered quantities (denoted by a tilde) as the continuity equation

$$\frac{\partial \widetilde{u}_i}{\partial x_i} = 0, \tag{2.1}$$

and momentum-conservation equation

Cases	Values	Non-Dim Number	Resolution
Changing R	20, **40**, 80, 160, 320 km	$Ro = V_g/Rf$	64^3, 128^3
Changing z_0	0.4,**0.410^{-2}**, 0.410^{-4} m	$Re = z_0 u*/\nu$	64^3, 128^3
Changing V_g	50, **60**, 70, 80 ms^{-1}	$Ro = V_g/Rf$	64^3, 128^3
Changing $\mathrm{d}V_g/\mathrm{d}R$	$-$(16.5, **33**, 42.3, 46.2)/R s^{-1}		64^3, 128^3
Changing $\mathrm{d}V_g/\mathrm{d}z$	0.1710^{-2} s^{-1}, **0.3310^{-2}** s^{-1}, 0.5010^{-2} s^{-1}	Baroclinicity strength $=(z_{Inflow}/u*)\mathrm{d}V_g/\mathrm{d}z$	64^3, 128^3
Changing the SGS models and their coeffcients	Three SGS models, and (0.5, 1.5) $\mathbf{c_{s,\Delta\,default}}$		64^3, 128^3

TABLE 1. Suite of the conducted LESs. The bolded values represent the default parameter values in each row.

$$\frac{\partial \widetilde{u}_i}{\partial t} + \widetilde{u}_j \left(\frac{\partial \widetilde{u}_i}{\partial x_j} - \frac{\partial \widetilde{u}_j}{\partial x_i} \right) = -\frac{1}{\rho}\frac{\partial \widetilde{p}^*}{\partial x_i} - \frac{\partial \tau_{ij}}{\partial x_j} + g\frac{\widetilde{\theta^*}'}{\theta_r}\delta_{i3} + f\widetilde{u}_2\delta_{i1} - \left[fV_g - \frac{\widetilde{u_2}^2}{r} + \widetilde{u}_1\frac{\partial U}{\partial r} + \frac{{V_g}^2}{r} \right]\delta_{i1} - f\widetilde{u}_1\delta_{i2} - \left[\frac{\widetilde{u}_1\widetilde{u}_2}{r} + \widetilde{u}_1\frac{\partial V}{\partial r} \right]\delta_{i2}, \tag{2.2}$$

where x_i is the position vector; $\widetilde{u}_i = (\widetilde{u_1}, \widetilde{u_2}, \widetilde{u_3}) = (\widetilde{u}, \widetilde{v}, \widetilde{w})$ is the resolved velocity vector in the (x, y, z) directions; $\tau_{\mathrm{ij}} = \sigma_{\mathrm{ij}} - 1/3\sigma_{\mathrm{kk}}\delta_{\mathrm{ij}}$ is the deviatoric part of the SGS stress tensor $\sigma_{\mathrm{ij}} = \widetilde{u_i u_j} - \widetilde{u_i}\,\widetilde{u_j}$; p^* is a modified pressure defined as $\widetilde{p}^* \equiv \widetilde{p} + 1/2\rho\widetilde{u}_j^2 + 1/3\rho\sigma_{\mathrm{kk}}$; f is the Coriolis parameter; δ_{ij} denotes the Kronecker delta; ρ is a constant fluid density; θ_r is a reference potential temperature; and g is the gravitational constant. The SGS deviatoric stress (τ_{ij}) is modeled using an eddy-diffusivity-type parameterization via the Lagrangian-averaged scale-dependent (LASD) dynamic Smagorinsky model (Bou-Zeid et al. 2005). More details about the neutral, baroclinic, and cyclonic simulation setups are presented by Momen & Bou-Zeid (2016), Momen (2022), Momen et al. (2018), and Momen et al. (2021). The terms in the bracket in Eq. (2.2) have been added specifically to simulate the HBL, where U and V denote the temporal average of the velocity in the radial and tangential directions, respectively. $\partial U/\partial r$ and $\partial V/\partial r$ are the large-scale velocity gradients in the radial direction, and V_g is the gradient wind. We used a direct Reynolds decomposition of the governing equations in a cylindrical coordinate to derive these terms (Momen et al. 2021), which allows us to retain all the relevant terms in their proper form. This method has been successfully validated against many observations over land and ocean (Momen et al. 2021).

2.1. *Suite of simulations*

A summary of all the conducted simulations is presented in Table 1. First, by varying the radius of the simulated portion of the hurricane from 20 km to 160 km, we investigate the effects of centrifugal forces (rotation) on the turbulent structures and mean flow dynamics of the hurricane. We characterized the effects of rotation using the Rossby number, $Ro{=}V_g/Rf$. The second sensitivity test was conducted by changing the aerodynamic roughness length, z_0, from 0.4 to 0.410^{-4} m. The relevant non-dimensional parameter is the Reynolds roughness number, defined as $Re{=}z_0 u*/\nu$, where $u*$ is the friction velocity and ν is the kinematic viscosity.

Next, we studied the effects of varying the gradient wind profile by changing the magnitude of V_g between 50 to 80 m/s and its gradients in both the vertical (z) and

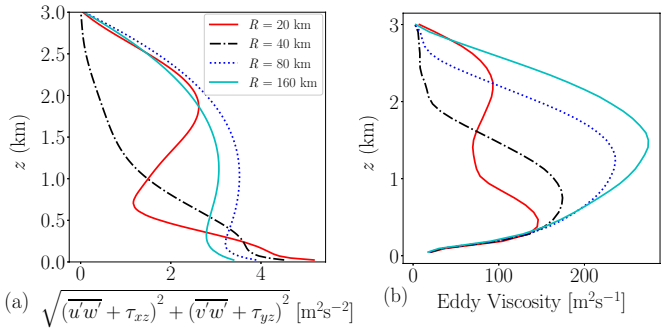

FIGURE 2. (a) Total Reynolds stress and (b) eddy-viscosity profile as a function of changing the radius or the Rossby number, $Ro = V_g/Rf$.

radial (r) directions. The details of the default quantities and multiplying coefficients for the gradient wind profiles are provided in Table 1. Finally, we conducted a set of simulations to study the effects of the SGS model on the turbulent structures of hurricanes by changing the Smagorinsky coefficient. All cases were simulated using both 64^3 and 128^3 grid resolutions with L_z=3 km, and L_x=L_y=$2\pi L_z$. In total, ([1 Default]+[4 R]+[2 z_0]+[3 V_g]+ [3 dV_g/dR]+[2 dV_g/dz]+[4 SGS])(2 resolutions)=38 LES cases were conducted.

3. Results and discussion

3.1. *The impacts of changing the Rossby number on Reynolds stresses and eddy viscosity*

Decreasing the distance of the simulation domain from the hurricane's center results in increased centrifugal forces. By investigating the total Reynolds stress profiles (resolved + SGS) for different radii shown in Figure 2(a), we notice that decreasing the radius or increasing Ro causes an increase in stresses near the surface. Increased rotation suppresses turbulence in the middle of the HBL and thus reduces the eddy viscosity. This effect can be seen in the HBL (for $z \lesssim 1.5$ km) in Figure 2(b). We note that as we decrease the radius, the eddy-viscosity profile becomes more non-monotonic (red line in Figure 2(b)). This can be potentially attributed to the fact that by further decreasing the radius, we are reaching the limit in where our transformation from the cylindrical to the Cartesian domain ($r \rightarrow x$ and $\theta \rightarrow y$) in the LES equations is valid.

3.2. *Characterizing the mean wind profiles via LES and a single-column model*

The rotation in HBLs impacts not only the turbulent fluxes but also the mean wind profiles. Increasing rotation suppresses the turbulence and decreases the turbulent boundary layer height in hurricanes. Figure 3(a) shows that as Ro increases the inflow layer height decreases. Furthermore, by increasing Ro, the maximum jet wind speed increases due to the suppression of turbulence. The height of this jet, which is correlated with the HBL height, also decreases with increasing Ro.

To further investigate the mean HBL dynamics, we developed a single-column model (SCM) by considering the following simplified HBL equations

$$\frac{\partial u_r}{\partial t} = \left(-fV_g - \frac{{V_g}^2}{R}\right) + fu_\theta + \frac{u_\theta^2}{R} + \frac{u_r^2}{R} + \frac{1}{\rho}\frac{\partial}{\partial z}(-\nu_T \frac{\partial u_r}{\partial z}), \tag{3.1}$$

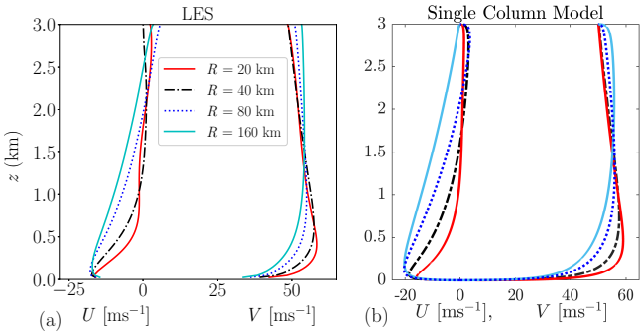

FIGURE 3. Wind profiles as a function of radius: (a) simulated by the LES and (b) estimated using a single-column 1D model and a prescribed eddy-viscosity profile.

Cases	R20	R40	R80	R160	R320
$Ro = V_g/Rf$	60	30	15	7.50	3.75
u_* [ms^{-1}]	2.266	2.117	1.969	1.837	1.734
z_{Inflow} [m]	∼750	∼1400	∼1950	∼2500	∼3000
z_{MaxVel} [m]	398.44	585.94	914.06	1734.37	2765.62

TABLE 2. Summary of the findings for changing Ro.

$$\frac{\partial u_\theta}{\partial t} = -f u_r - u_r \frac{\partial V_g}{\partial R} - \frac{u_\theta u_r}{R} + \frac{1}{\rho}\frac{\partial}{\partial z}(-\nu_T \frac{\partial u_\theta}{\partial z}), \tag{3.2}$$

where u_θ and u_r are the tangential and radial velocity, f denotes the Coriolis frequency (510^{-5} s^{-1} here), and ν_T is the eddy viscosity. For the eddy viscosity, we employed a similar profile to O'Brien's profile (O'Brien 1970). Using this analytical eddy-viscosity profile formula, which is similar to Figure 2(b), we can close Eqs. (3.1)-(3.2) and solve the governing partial differential equations numerically. The wind profiles from the SCM are in good agreement with the LES results (compare Figure 3(a,b)). Therefore, a 1D simple numerical model with an appropriate eddy-viscosity formulation can reproduce the mean flow dynamics in HBLs. We plan to use this SCM to characterize the impacts of vertical advection on HBL dynamics in future work.

The impacts of Ro on inflow layer depth and friction velocity are summarized in Table 2 using these simulations. The z_{Inflow} is defined as the height in which $u_r \sim 0$ for the first time and is estimated from Figure 3(a). The z_{MaxVel} is also defined as the height of the maximum jet velocity and is determined from Figure 3(a). The results in Table 2 indicate that by increasing Ro,, the z_{Inflow} and z_{MaxVel} decrease and the jet maximum velocity and consequently the friction velocity, u_*, increase.

3.3. *The impacts of the Rossby number on coherent turbulence structures*

In this section, we determine the impacts of changing Ro on coherent turbulence structures. Figure 4 shows the instantaneous velocity fields for two values of Ro. Figure 4(a) depicts the turbulence structures for R=40 km, and Figure 4(b) displays the results for R=160 km. To quantify the size and orientation of the dominant eddies inside the hurricane, we calculated the 2D spatial correlation of the velocity. As the figure indicates, at

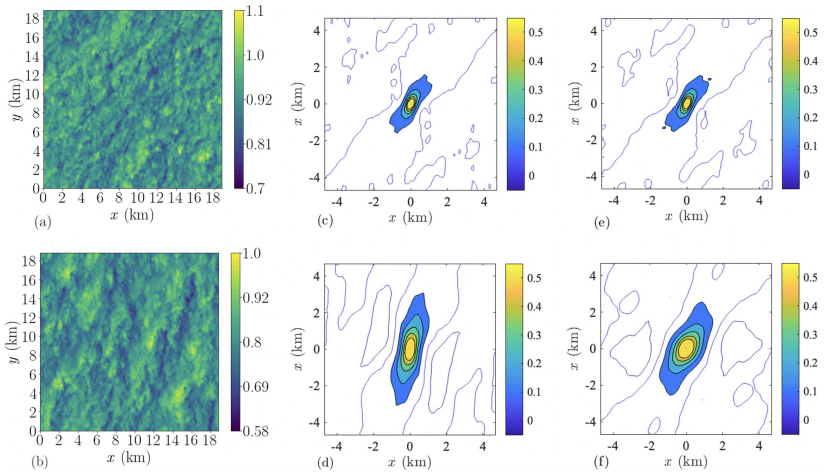

FIGURE 4. The normalized instantaneous wind contours at 300 m height from the surface for a radius of (a) 40 km and (b) 160 km. (c-f) The 2D spatial correlation corresponding to the wind contours at different elevations for (c) $R = 40$ km and (d) $R = 160$ km at $z = 300$ m, and for (e) and (f) at the non-dimensional height of $z = z_{maxVel}/2$.

the same physical elevation above the surface (300 m), increasing *Ro* decreases the size of the coherent eddies and alters their orientation (compare Figure 4(c,d)). To investigate whether this conclusion holds for non-dimensional elevations, we rescaled the height with z_{MaxVel} and showed the spatial correlations at z=1/2 z_{MaxVel} for both cases. The results from Figure 4(e,f) demonstrate that the orientation of the eddies is similar for these two values of *Ro* at the same non-dimensional height. Nevertheless, the size of the eddies still appears to be different. We also tested different rescaling methods such as using z_{MaxVel} and u_*/f for non-dimensionalizing the size of the eddies, but they still did not collapse. This underscores the need for a proper scaling for the size of coherent turbulent eddies in HBLs.

To comprehensively assess the impacts of *Ro* on the size and orientation of turbulent eddies, we performed the spatial correlation for 30 snapshots of wind contours at each elevation for each case. Then, we fitted an ellipse to the spatial correlation contours (correlation = 0.3) in Figure 4(c-f). The size of the eddies is estimated as $\sqrt{a^2 + b^2}$, where a is the major axis and b is the minor axis. The orientation of the eddies is also calculated based on the angle of the major axis of this ellipse. The results for the four cases at the same non-dimensional height are depicted in Figure 5. As the figure indicates, increasing *Ro* or rotation (decreasing the radius) leads to a decrease in the size of the eddies. The orientation of the eddies at half of the jet's maximum velocity (z_{MaxVel}) remains relatively the same for the considered cases.

3.4. *The impacts of changing the Rossby number on TKE budget profiles*

Next, we examined the turbulent kinetic energy (TKE) budget profiles as a function of *Ro*. The TKE budget terms are defined as follows in our LES

$$SP \equiv -\overline{u'w'}\frac{\partial \overline{u}}{\partial z} - \overline{v'w'}\frac{\partial \overline{v}}{\partial z} = (\overline{u}\ \overline{w} - \overline{uw})\frac{\partial \overline{u}}{\partial z} + (\overline{v}\ \overline{w} - \overline{vw})\frac{\partial \overline{v}}{\partial z}, \tag{3.3}$$

$$RT \equiv -\frac{\partial \overline{w'e}}{\partial z} = -\frac{1}{2}\frac{\partial}{\partial z}(\overline{u^2 w} - 2\overline{u}\ \overline{uw} + \overline{v^2 w} - 2\overline{v}\ \overline{vw} + \overline{w^3}), \tag{3.4}$$

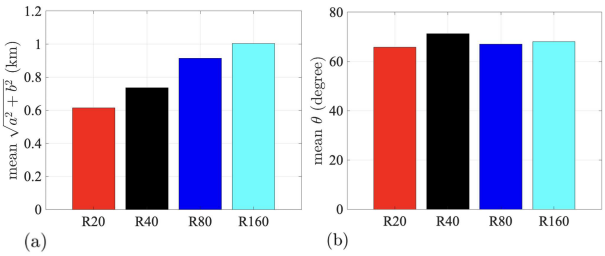

FIGURE 5. The spatial correlation analysis as a function of the Rossby number at a non-dimensional height of $z = z_{MaxVel}/2$. The results are calculated from the fitted ellipse to the spatial correlations in Figure 4, representing (a) the size and (b) the orientation of the eddies.

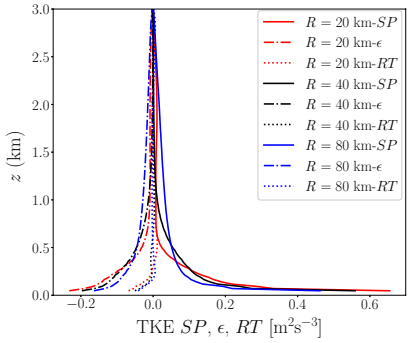

FIGURE 6. TKE budget profile of HBLs as a function of *Ro*.

$$\varepsilon \equiv \overline{\tau'_{ij} S'_{ij}} = \overline{\tau_{ij} S_{ij}} - \overline{\tau_{ij}}\ \overline{S_{ij}}, \tag{3.5}$$

where SP, RT, and ε are shear production, resolved turbulent transport, and SGS dissipation, respectively. More details about the TKE budget dynamics and its calculation in our LES are presented by Momen & Bou-Zeid (2017) and Momen et al. (2018). As we increase the radius (decrease *Ro*), the near-surface values of the shear production term (solid lines in Figure 6) decrease, similar to the u_* values in Table 2. However, away from the wall (approximately $z > z_{MaxVel}$), the effects of the centrifugal forces and rotation become larger, and the shear production decreases with decreasing *Ro*. Resolved transport and dissipation terms show similar behavior.

3.5. *Changing z_0*

The results of all other sensitivity tests are shown next. A summary of the main findings from each test is presented in Table 3. The next sensitivity test we investigated is for changing z_0 in HBLs. As Figure 7 shows, the default z_0 is 0.004 m, and we considered two additional cases (100 times rougher and smoother) to conduct a sensitivity test. We can see that increasing z_0 leads to enhanced turbulent stresses (Figure 7(b)), increased inflow layer and HBL height (Table 3), and lower maximum jet velocities (Figure 7(a)) as expected. The proper selection of z_0, especially by considering air-sea interactions and ocean waves at these high wind speeds, is thus critical for accurate predictions of HBL wind profiles.

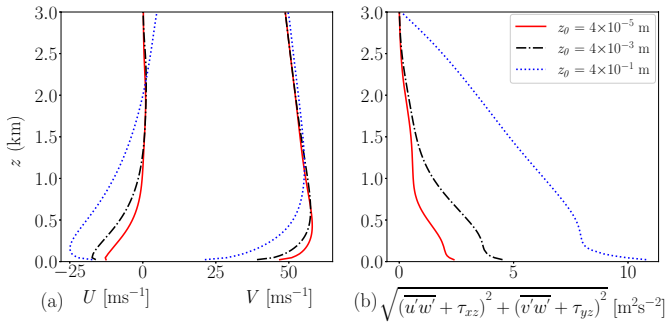

FIGURE 7. (a) Wind profile and (b) total Reynolds stress by changing z_0 in the HBL.

3.6. *Changing V_g, dV_g/dz, and dV_g/dR*

We examined the effects of changing the magnitude and shape of the imposed gradient wind profile on the hurricane dynamics. Increasing the magnitude of the imposed gradient wind (V_g) leads to an increase in $Ro = V_g/Rf$. The impacts are thus similar to reducing the radius, leading to a lower HBL height and an increased u_* (see Table 3). Changing the vertical gradient of the V_g ($\mathrm{d}V_g/\mathrm{d}z$ or baroclinicity strength) alters the HBL height but not the u_* at the surface as expected. This is because the imposed V_g at the surface remains the same while its vertical gradient changes. Increasing the baroclinicity strength leads to a shallower HBL height, as shown in Table 3. We also imposed different values of the radial velocity gradient by multiplying the default value by different coefficients. The value of the $\mathrm{d}V_g/\mathrm{d}R$ appears to have a similar impact on the result as Ro. Decreasing the magnitude of $\mathrm{d}V_g/\mathrm{d}R$ leads to lower Reynolds stresses and thus a higher maximum jet velocity and a lower HBL.

Cases	Changed Variable	Non-Dim. Number	u_* [ms^{-1}]	z_{Inflow} [m]	z_{MaxVel} [m]
Changing z_0	410^{-1} m	Re_1= 78,142	3.280	~2000	1125
$Re = z_0 u_*/\nu$	410^{-3} m	Re_2= 502.9	2.117	~1400	586
	410^{-5} m	Re_3= 3.67	1.540	~1100	398
Changing V_g	50 ms^{-1}	25	1.745	~1750	703
$Ro = V_g/Rf$	60 ms^{-1}	30	2.117	~1400	586
	80 ms^{-1}	40	2.856	~1250	516
Baroclinicity strength=	0.17 10^{-2} s^{-1}	1.077	2.130	~1350	656
$(z_{Inflow}/u_*)\mathrm{d}V_g/\mathrm{d}z$	0.33 10^{-2} s^{-1}	2.182	2.117	~1400	586
	0.50 10^{-2} s^{-1}	3.921	2.104	~1650	540
$\mathrm{d}V_g/\mathrm{d}R$ R/V_g	-16.5 [ms^{-1}] $/R$	-0.275	2.156	~1100	445
	-33 [ms^{-1}] $/R$	-0.550	2.117	~1400	586
	-46.2 [ms^{-1}] $/R$	-0.770	2.066	~2400	1687

Table 3: Summary of the findings from parameter sensitivity tests for z_0 and V_g.

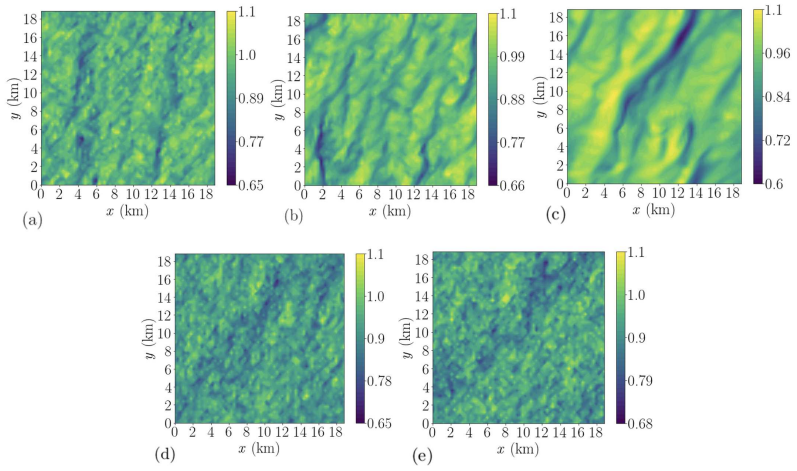

FIGURE 8. Normalized tangential velocity wind contour by V_g for different Smagorinsky coefficients: (a) $0.5c_{s,\Delta,\text{default}}$, (b) $c_{s,\Delta,\text{default}}$, and (c) $2c_{s,\Delta,\text{default}}$. The results are for (a-c) the static Smagorinsky SGS model, (d) the dynamic Smagorinsky model, and (e) the LASD model.

3.7. *Changing the Smagorinsky coefficient*

Finally, we examined the effects of changing the LES SGS model on hurricane turbulence structures. The Smagorinsky model for calculating the SGS stress tensor is defined as

$$\tau_{\text{ij}}^{\text{SMAG}} = -2\nu_T \widetilde{S}_{\text{ij}} = -2(c_{s,\Delta}\Delta)^2 \left|\widetilde{S}\right| \widetilde{S}_{\text{ij}}, \tag{3.6}$$

where $c_{s,\Delta}$ denotes the Smagorinsky coefficient, and $\widetilde{S}_{\text{ij}}$ and $\left|\widetilde{S}\right|$ are the strain-rate tensor and strain-rate magnitude, respectively. We tested static and dynamic Smagorinsky model as well as an LASD dynamic Smagorinsky model (Bou-Zeid et al. 2005). We also varied the magnitude of the default $c_{s,\Delta}$ in the static Smagorinsky model by multiplying it by different values. The mean wind profiles were not significantly sensitive to changes in the Smagorinsky coefficient (not shown); however, this change strongly affected the coherent turbulence structures. Figure 8 indicates that as we increase the Smagorinsky coefficient (SGS stress), turbulence is dissipated more. Thus, the turbulence decreases in the HBL flow and the size of the eddies becomes larger (compare Figure 8(a-c)) The regular dynamic Smagorinsky model and the LASD model do not show considerable differences in the structure of turbulent eddies in this rotating flow (compare Figure 8(d,e)). However, it appears that the default static model (Figure 8(b)) is more dissipative than these dynamic SGS models. It thus produces less turbulent eddies in the HBL than dynamic Smagorinsky models. These results underscore the significance of the LES SGS models for the structure of coherent turbulent eddies in HBLs.

4. Conclusions

In total, 38 new LESs of HBLs were carried out by varying the HBL parameters, such as Rossby number, roughness Reynolds number, and baroclinicity strength. Our key findings from this study are summarized below.

Increasing *Ro* increases the HBL jet magnitude, suppresses turbulence, decreases the

size of turbulent eddies, and changes their orientation at the same elevation. Increasing *Ro* essentially acts to increase the effective Coriolis parameter, which reduces the Ekman depth. If the largest eddies scale with the Ekman depth, then their length scale is expected to shrink with R. Furthermore, u_* and turbulence shear production are enhanced near the wall by increasing *Ro* while they decrease away from the wall (approximately above z_{MaxVel}), where the centrifugal forces effects become larger.

With an appropriate eddy viscosity from LES, an SCM can capture the overall mean flow dynamics of HBLs when compared with the LES. Increasing V_g leads to increased *Ro* and thus has a similar impact on HBLs. Increasing the magnitude of the vertical gradient of the gradient wind ($|\mathrm{d}V_g/\mathrm{d}z|$ or baroclinicity strength) leads to a shallower HBL height, but it does not impact the u_* at the surface since the imposed gradient wind at the surface remains the same.

Larger Smagorinsky coefficients increase the eddy diffusivity and, therefore, further dissipate the turbulence and leave mostly larger turbulent structures. The static Smagorinsky model appears to be more dissipative than the dynamic SGS models and generates fewer small turbulent eddies.

Acknowledgments

The simulations were performed on the Carya cluster at the University of Houston.

REFERENCES

Emanuel, K., 2005 Increasing destructiveness of tropical cyclones over the past 30 years. *Nature* **436**, 686–688.

Bou-Zeid, E., Meneveau, C., & Parlange, M., 2005 A scale-dependent Lagrangian dynamic model for large eddy simulation of complex turbulent flows. *Phys. Fluids* **17**, 025105.

Bryan, GH., Worsnop, RP., Lundquist, JK., & Zhang, JA., 2017 A simple method for simulating wind profiles in the boundary layer of tropical cyclones. *Bound. Lay. Meteorol.* **162**, 475–502.

Green, BW., & Zhang, F., 2015 Idealized large-eddy simulations of a tropical cyclonelike boundary layer. *J. Atmos. Sci. 72,* 1743–1764.

Momen, M., 2022 Baroclinicity in stable atmospheric boundary layers: characterizing turbulence structures and collapsing wind profiles via reduced models and large-eddy simulations. *Q. J. Roy. Meteor. Soc.* **148**, 76–96.

Momen, M., & Bou-Zeid, E., 2016 Large eddy simulations and damped-oscillator models of the unsteady Ekman boundary layer. *J. Atmos. Sci.* **73**, 25–40.

Momen, M., & Bou-Zeid, E., 2017 Mean and turbulence dynamics in unsteady Ekman boundary layers. *J. Fluid Mech.* **816**, 209–242.

Momen, M., Bou-Zeid, E., Parlange, MB., & Giometto, M., 2018 Modulation of mean wind and turbulence in the atmospheric boundary layer by baroclinicity. *J. Atmos. Sci.* **75**, 3797−3821.

Momen, M., Parlange, MB., & Giometto, MG., 2021 Scrambling and reorientation of classical boundary layer turbulence in hurricane winds. *Geophys. Res. Lett.* **48**, e2020GL091695.

O'Brien, JJ., 1970 A note on the vertical structure of the eddy exchange coefficient in the planetary boundary layer. *J Atmos Sci* **27**, 1213–1215.

Romdhani, O., Zhang, JA., & Momen, M., 2022 Characterizing the impacts of turbulence closures on real hurricane forecasts: a comprehensive joint assessment of grid resolution, horizontal turbulence models, and horizontal mixing length. *J. Adv. Model. Earth Sy.* **14**, e2021MS002796.

Zhang, S., Pu, Z., & Velden, C., 2018 Impact of enhanced atmospheric motion vectors on HWRF hurricane analyses and forecasts with different data assimilation configurations. *Mon. Weather Rev.* **146**, 1549–1569.